Hierarchical porous carbon derived from covalent triazine frameworks for high mass loading supercapacitors

Daniel Baumann, Chain Lee, Chengzhang Wan, Hongtao Sun, Xiangfeng Duan

Department of Chemistry and Biochemistry, University of California, Los Angeles, California 90095, United States

ABSTRACT: Here we report a straightforward approach to synthesize hierarchical porous carbon (HPC) via a high temperature ionothermal synthesis and partial pyrolysis of a covalent triazine framework (CTF) in molten $ZnCl_2$. By using 1,4 dicyanobenzene (DCB), 1,3-dicyanobeznene (mDCB), or 2,6-dicyanopyradine (DCP) as the monomer precursor for the CTF, we found that $ZnCl_2$ acts as an effective porogen in the system for monomers with weak solvent-solute interactions (DCB and mDCB). The resulting HPCs derived from DCB and mDCB exhibits a systematically tunable hierarchical porosity with an average pore size ranging from 2.5 - 8 nm, by varying the concentration of monomer in solution. We show a decreasing DCB:$ZnCl_2$ ratio gives rise to larger mesopores, with improved pore connectivity and accessibility that is beneficial to mass transport and ion diffusion for high performance electric double layer capacitors (EDLCs) at high mass loadings. We demonstrate EDLCs with specific capacity values over 155 F/g at high mass loadings of 15 mg/cm^2, and exceptional areal capacities of over 2.27 F/cm^2 at low rates and 1.48 F/cm^2 at high rates.

Energy storage is becoming more important than ever as the world's demand for portable energy rapidly increases. Many electronic devices require components that can handle large power spikes, with fast charge and discharge rates (seconds to minutes) like electric vehicles, laptops, and backup power generators.[1,2] Electric double layer capacitors (EDLCs) are attractive for fulfilling such technological needs, through their exceptional power densities and robust cyclability.[2]

These unique high power characteristics of EDLCs are attributed to their fundamental operating mechanism – the electrical double layer effect. Capacitance originates from the separation and absorption of charged ions on the surface of the electrodes.[1-4] This process is non-faradaic and only limited by electrolyte diffusion in the electrode, which promises very high charge and discharge rates with unrivaled stability, but often with a limited capacity due to the nature of surface ion absorption. The capacity of EDLCs is directly tied to the surface area of the electrode. More surface area means more ions can be adsorbed, resulting in higher capacities. Tremendous effort has gone into improving the capacity values.

In this regard, carbonaceous materials are particularly attractive for their high surface areas as well as excellent electrochemical stability.[2,5] In particular, nanostructured carbon materials have shown great potential for boosting the capacities of supercapacitor electrodes. For example, microporous carbon electrodes have shown high capacities of over 250 F/g at high rates.[2,5] However, the areal mass loading of the electrodes is often overlooked, and is typically very small (0.5 – 1.0 mg/cm^2). In this case, if one takes the mass of the entire device into consideration (casing, current collector, separator, etc.), the overall capacity of the devices with such low mass loadings is seriously compromised. Realistic loadings of the active materials with a total mass comparable to that of the current collector (~ 10 mg/cm^2) are necessary for practical applications. However, the performance of many supercapacitor materials reported to date drops quickly as the electrodes become thicker at higher mass loading. This is due to many factors, such as increased internal resistance of the electrode and poor ion diffusion through thicker electrodes.[6] Developing nano architectured materials to maintain their outstanding performance at practical mass loadings is crucial for the development and application of high performance supercapacitors.

A good candidate for supercapacitor active materials are covalent organic frameworks (COFs). They feature several desirable characteristics of a supercapacitor material, including high surface areas, tunable porosities, and diverse functional groups.[7,8] However, typical COFs lack high electrical conductivity, which is essential for EDLC function.

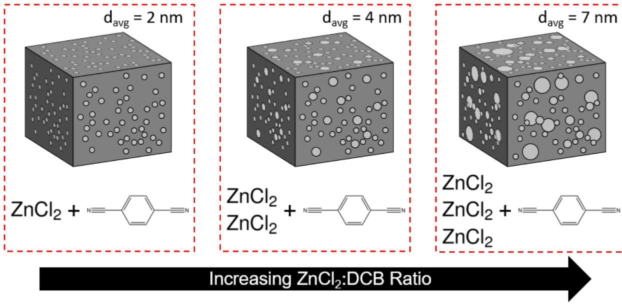

Figure 1. The porosity evolution in the CTF-derived HPCs with varying $ZnCl_2$ to DCB ratios. Small micropores are maintained for high surface area, while larger mesopores are created to ensure efficient ion diffusion throughout the material.

Solutions to this problem are mostly achieved through pyrolysis/carbonization of the COF[9,10] or synthesizing the COF in the presence of a conductive host material[11]. Another potential way to enhance conductivity is to use conjugated monomers.[12–14] To this end, covalent triazine framework (CTF) represents a unique class of COFs with a fully conjugated structure.

Pioneered by Kuhn *et al.*, these CTFs contain a triazine motif with high surface area, and are synthesized from cheap, abundant aromatic nitriles.[15,16] The conjugated CTFs fulfill all of the necessary attributes for use in energy storage due to their high surface areas, moderate electrical conductivity, high chemical/physical stability, and tunable geometries.[12,16] Additionally, the rich nitrogen groups in CTFs may also be beneficial to EDLCs through enhanced wettability of the electrolyte, introduction of pseudocapacity (aqueous electrolytes), and increased active surface area.[17] Hao *et al.* first reported CTFs for supercapacitor applications by using a high nitrogen content monomer unit and a high temperature synthesis to generate a mesoporous framework with desirable high surface area and conductivity.[12]

Here, we focus on developing tunable hierarchical porous frameworks that contain both micropores and mesopores to allow for efficient ion diffusion while still maintaining a high surface area. This is crucial for high rate and high loading devices. Hierarchical porous carbon (HPC) with modest nitrogen content (~ 7 – 9 at%) was generated through the high temperature ionothermal synthesis and partial pyrolysis of a CTF in molten $ZnCl_2$. By tailoring the 1,4-dicyanobenzene (DCB) monomer precursor concentration in the $ZnCl_2$ melt, HPCs can be readily produced with widely tunable pore size distributions. With a tunable hierarchical porosity for highly efficient ion transport, we show the resulting HPCs can be used for constructing EDLCs with specific capacity values over 155 F/g at a high mass loading of 15 mg/cm^2, and exceptional areal capacities of over 2.27 F/cm^2.

Synthesis and Characterization of HPCs. The HPCs were synthesized from the trimerization reaction of 1,4-dicyanobenzene (DCB) in a molten $ZnCl_2$ salt. In a typical synthesis, 400 mg of DCB and the desired weight of $ZnCl_2$ were ground together in a pestle and mortar inside of a glovebox. The resulting mixture was transferred to a quartz ampoule, evacuated, and sealed. The samples were heated to 700 °C in one hour, and reacted for 20 hours. After cooling to room temperature, a large black monolith was obtained, which was ground and then washed with a 0.5 M HCl solution three times, water once, and THF twice. The washed sample was dried in a vacuum oven at 120 °C overnight. The same method was also used to prepare HPCs using 1,3-dicyanobeznene (mDCB), or 2,6-dicyanopyradine (DCP) monomers for mechanism studies.

The morphology of the samples was studied by scanning electron microscopy (SEM), using a JEOL JSM-6700F FE-SEM at 8 kV. Energy dispersive X-ray (EDAX) spectroscopy was obtained from a METEK Z2e analyzer at 10 kV and a probe current of 15 µA. Transmission electron microscopy (TEM) was performed using a FEI T12 operated at 120 kV.

N_2 adsorption-desorption isotherms were obtained at 77 K using a micromeritics TriStar 3020. Samples were degassed at 175 °C under vacuum overnight before measurements. Surface areas were calculated from Brunauer-Emmett-Teller (BET) theory, and pore size distributions were obtained through density functional theory (DFT).

Raman spectroscopy experiments were performed on the HPCs using a Horiba LabRam HR800 system with an excitation wavelength of 514 nm.

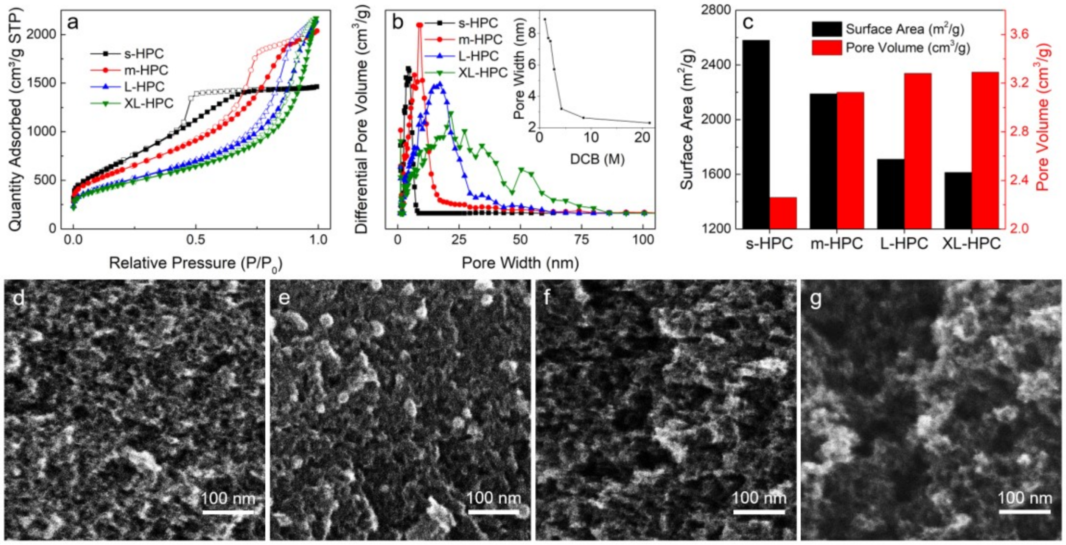

Figure 2. BET isotherm (a) and differential pore volume (b) plots shows hierarchical porosity of the samples prepared with different monomer:$ZnCl_2$ ratios denoted s, m, L, and XL-HPC for increasing pore size distribution. The inset in (b) shows that the average pore size is directly correlated to the concentration of DCB in solution, reaching a minimum at around 2.5 nm. The hysteresis in the isotherm plot is indicative of mesoporous samples. A summary of the surface area and pore size are shown in (c). The SEM images of s-HPC (d), m-HPC (e), L-HPC (f), and XL-HPC (g) show an increasing pore size in the resulting HPCs.

Powder X-ray diffraction (XRD) was performed on a Bruker D8 with Cu Kα x-rays (λ = 0.15418 nm). The step size was 0.014° every 0.18 s operated at 45 V and 10 mA.

A composite was made for EDLC testing. This was achieved by mixing the desired HPC, conductive carbon (Super P), and polytetrafluoroethylene (PTFE) together in a 7:2:1 by weight ratio in an agate mortar, respectively. Water was added to create a free standing film, which was pressed at various thicknesses. Samples were dried in a vacuum oven at 120 °C overnight, cut into circular electrodes with a diameter of 4 mm, then immersed in an ionic liquid electrolyte, 1-ethyl-3-methylimidazolium tetrafluoroborate ($EMIMBF_4$). The symmetric cell was made by pressing two electrodes between 2 gold coated glass slides with a Whatman ashless filter paper as the separator.

Cyclic voltammetry (CV), galvanostatic charge-discharge (GCD), and electrochemical impedance spectroscopy (EIS) were obtained from a CHI760e using symmetric double cells. Specific capacity (C_s, F/g) is measured from the GCD using $C_s = 2It/mV$, where I is the discharge current, t is the discharge time, m is the mass of HPC in a single electrode, and V is the potential window. Device capacities (C_{all}, F/g_{all}) are calculated by incorporating inert components utilizing the formula $C_{all} = C_s/(1+\sigma_{inert}/\sigma_A)$ where σ_{inert} is the inert component's mass loading (chosen to be 10 mg/cm^2) and σ_A is the mass loading of the HPC. Areal capacity (C_A, F/cm^2) is calculated as $C_A = C_s{*}\sigma_A$. Energy (E, Wh/kg) is determined using $E = \frac{1}{8}C_sV^2$ and power (P, W/kg) is found with P = E/t.

Physical and chemical properties. The high temperature synthesis of DCB has been proven to increase surface area, porosity, and conductivity of the resulting CTF.[12] By further tuning the reaction conditions, hierarchically porous carbon (HPC) was obtained from the simultaneous synthesis and pyrolysis of the CTF at 700 °C. The DCB to $ZnCl_2$ molar ratio was varied from 1:1 to 1:20 to create the various HPCs (Figure 1). Of the samples obtained with this method, four with significantly different pore size distributions were chosen for characterization and electrochemical studies. From the smallest pore size to the largest, the samples are denoted s, m, L, and XL-HPC, corresponding to HPCs obtained with DCB:$ZnCl_2$ ratios of 1:5, 1:7.5, 1:12.5, and 1:20, respectively.

N_2 adsorption and desorption isotherms were used to determine the surface characteristics of the HPCs (Figure 2a). The adsorption-desorption curves take the shape of a type IV isotherm, indicating the presence of both micropores and mesopores in each HPC. Furthermore, the hysteresis loop gradually shifts from H2 to H3 type as the ratio of $ZnCl_2$ gets higher (Figure 2a), indicating the change from "ink bottle" pores to slit like pores.[18] This is most likely due to the $ZnCl_2$ acting as a porogen during the synthesis, as also postulated previously.[19,20] The differential pore size distributions for the series of samples are further shown in Figure 2b. It is apparent that the s-HPC obtained with the DCB:$ZnCl_2$ ratio of 1:5 shows limited hierarchical porosity. With an increasing ratio of $ZnCl_2$, the pores expand dramatically, with an average pore diameter shift from 2.5 nm in s-HPC to almost 10 nm in XL-HPC (Figure 2b). One important aspect of the differential pore volume plots is the preservation of small pores (0.5 – 2 nm) in the structure, which are essential for retaining high surface while hierarchical porosity is being introduced with the increasing $ZnCl_2$ ratio.

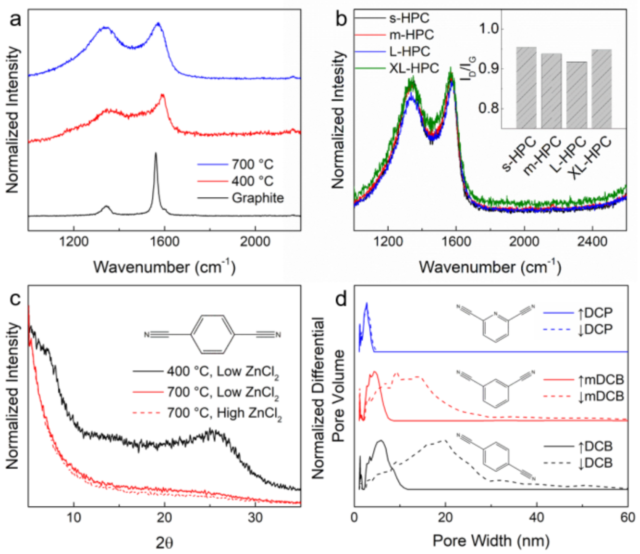

Figure 3. Raman spectra of the high temperature synthesis shows an I_D/I_G ratio of around 1, which is consistent for amorphous carbon (a). Each HPC has a I_D/I_G ratio of around 1 (b), meaning $ZnCl_2$ did not enhance pyrolysis, but acted as a porogen. XRD of DCB indicates no graphitization of the sample, and that it is mostly amorphous, losing any periodicity (c). The differential pore volume is dictated not only by the $ZnCl_2$ content, but also the monomer used (d). Both mDCB (red) and DCB (black) show expanded pore sizes at high monomer:$ZnCl_2$ ratios, while DCP (blue) is unchanged.

SEM images confirm the porosimetry results, showing a gradual shift from small pores to large pores (Figure 2d-g). Comparing the smallest sample, s-HPC (Figure 2d), to the largest, XL-HPC (Figure 2g), one can see the stark difference in the porosities. No large voids are seen in s-HPC and the surface is relatively uniform, confirming the limited hierarchical porosity as shown in the pore size distribution plot. Figure 2g especially demonstrates the hierarchical nature of the larger HPCs. There are large cavernous voids dotted with small pores along the walls. This interconnected network of pores is critical for efficient mass transport and electrolyte penetration to ensure pore accessibility. TEM studies also confirm a similar evolution of the porous structures in these different samples (Figure S1). It is noted that the larger pore size comes at a cost of surface area. The s-HPC has a surface area of 2581 m^2/g, while the XL-HPC has a ~ 40% reduction in surface area to 1614 m^2/g.

Raman spectroscopy was used to characterize the HPCs. The main peaks of interest are the D-peak (1360 cm^{-1}) which arises from sp^2 hybridized carbon's breathing mode and G-peak (1560 cm^{-1}) is due to the bond stretching of all sp^2 hybridized carbon.[21,22] These can be used to approximate the degree of sp^2 and sp^3 carbon in a sample.[22,23] Carbon samples that are highly graphitized have a low I_D/I_G ratio, while amorphous carbons have a much higher I_D/I_G ratio (ranging from 0.8 – 1.5). Figure 3a shows the contrast

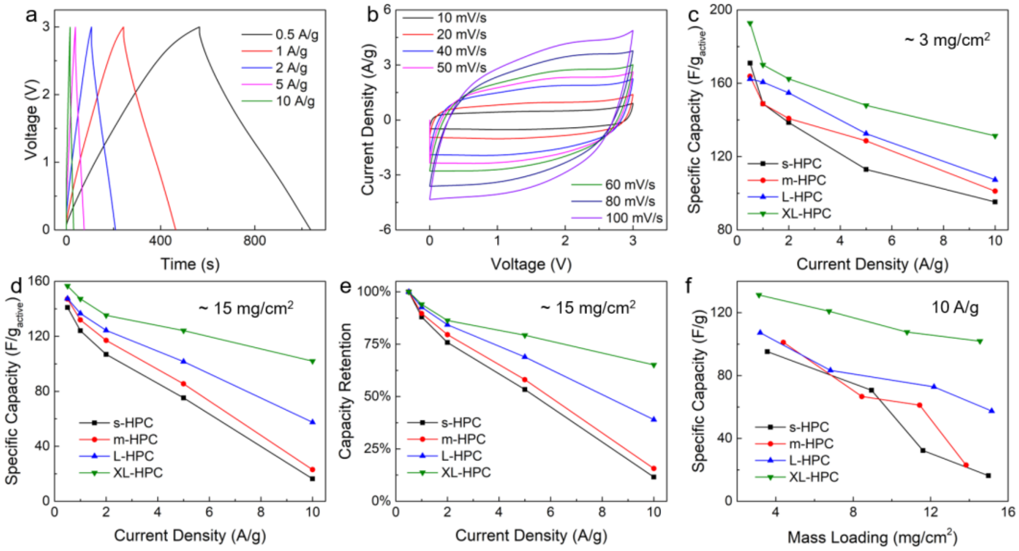

Figure 4. GCD (a) and CV (b) of a typical HPC. Capacity vs current density plots of each HPC at 3 mg/cm^2 (c) and 15 mg/cm^2 (d). HPCs with a larger pore size distribution show enhanced capacity retention for high loading (e). Capacity vs mass loading at 10 A/g displays the effectiveness of each HPC as loading is increased (f).

between graphite with a low I_D/I_G ratio, and CTFs synthesized at different temperatures. The 400 °C CTF (referred to as CTF-1 in literature) has been shown to stack similar to graphite but with limited periodicity.[15] This leads to an increased I_D/I_G ratio as compared to graphite. The 700 °C sample exhibits an even higher ratio, indicating the structure lacks periodicity, and is mainly amorphous. Figure 3b shows that the HPCs with different pore size each have an I_D/I_G ratio of around 1, which is consistent with other amorphous carbons.[4,10,17,22] The similar ratios indicate that each sample has roughly the same degree of amorphous character, suggesting that the amount of $ZnCl_2$ did not significantly affect the pyrolysis.

The XRD patterns provide further evidence of the amorphous nature of the HPCs. Comparing CTF-1 to the higher temperature displays the difference in structure. As stated previously, CTF-1 has a layered structure that lacks long range periodicity. This broadens the (001) stacking XRD peak at around 26°, as seen in Figure 3c.[24] The (001) stacking peak disappeared during the higher temperature synthesis at both low and high $ZnCl_2$ concentrations, which may be attributed to N crosslinking throughout the structure.[12,16]

To probe whether or not the monomer geometry affected the resulting porosity, we have explored two other monomer units for the synthesis under the same reaction conditions. DCB and its meta isomer, mDCB, showed similar behavior at low and high $ZnCl_2$ amounts (Figure 3d). The differential pore volume plots show that at high $ZnCl_2$ amounts hierarchical porosity is introduced. In contrast, the pyridine containing monomer DCP showed no such pore expansion. The low and high ratio samples had identical pore size distributions. The solvent-solute interaction is suspected to be stronger for DCP than mDCB and DCB due to the presence of a pyridine. This stronger interaction may prevent the $ZnCl_2$ from creating mesopores in the structure because it is "locked" in place inside the CTF structure.[16] The weaker interaction with DCB and mDCB may allow for free $ZnCl_2$ to occupy a large volume between growing CTF sheets giving rise to hierarchical porosity. This further suggests that $ZnCl_2$ is acting as a porogen in the HPC system rather than enhancing pyrolysis of the overall structure. EDAX analysis supports this conclusion because each HPC contains a similar nitrogen amount of 8 – 10 wt% (Table S1). If $ZnCl_2$ promoted hierarchical porosity through pyrolysis there would be a defined loss in N content with increasing $ZnCl_2$ amount.

This combined evidence suggests that the hierarchical porosity results from porogen effects rather than degradation. It is crucial to understand these interactions, because some monomers will not produce hierarchical porosity. To enhance nitrogen content, different monomers with weaker solvent-solute interactions should be chosen, particularly ones lacking a pyridine motif.

EDLCs and Electrochemical properties. To assess the electrochemical properties of the HPCs, EDLCs were made and tested by cyclic voltammetry (CV), galvanostatic charge-discharge (GCD), and electrochemical impedance spectroscopy (EIS). Figure 4a & b show a typical GCD and CV, respectively. Figure 4c represents the capacitance vs. current density at a low loading (3 mg/cm^2) of each HPC. It can be seen that at lower mass loadings the samples are relatively similar, with little capacity degradation comparable to that of other carbon materials using ionic liquids as the electrolyte.[3,25] At low current densities and low loading the highest capacities are achieved. At 0.5 A/g with a loading of 3 mg/cm^2 the s, m, L, and XL-HPCs exhibited similar gravimetric (specific) capacities of 171 F/g, 163 F/g, 162 F/g, and 192 F/g, respectively. At this current density, the surface area is more impactful for the smaller HPCs, as s-HPC (2581 m^2/g) has a higher capacitance over m-HPC

($2189 m^2/g$); both of which have similar pore size distributions. However, L-HPC ($1711 m^2/g$) and XL-HPC ($1614 m^2/g$) appear to overcome their low surface area with increased pore accessibility from the hierarchical porous structure as both have lower surface area than s & m-HPC, but rise in capacity. At a higher current density of 10 A/g, the benefit of the hierarchical porosity becomes more evident as the overall capacities for different HPCs drop to 95 F/g (s-HPC), 101 F/g (m-HPC), 107 F/g (L-HPC), and 131 F/g (XL-HPC). Here the importance of the hierarchical porosity in facilitating more efficient mass transport is clearly manifested, as the samples with the larger pore sizes show higher capacities, as well as a smaller drop in capacity. XL-HPC achieves the highest capacity of 192 F/g, representing the highest value achieved in a CTF derived carbon in a symmetric cell.[12] At a loading of 3 mg/cm^2 with an ionic liquid electrolyte, this data is on par with that of literature values that have capacities ranging from 150-200 F/g at low current densities.[25–29] Electrodes also show moderate stability with 85% capacity retention over 8000 cycles (Figure S2).

At high mass loadings, the capacities differ substantially. An expected drop in specific capacity is observed for all electrodes, due to larger resistances and ion transfer distances in thicker electrodes (Figure 4d).[30] Nonetheless, it is apparent that the samples with the larger pores better retain their capacities and rate performance when compared to that of the smaller pore HPCs, demonstrating that the larger pore samples are able to cope with high currents at high loading much better than that of their smaller pore counterparts. At a low rate of 0.5 A/g each HPC has a capacity around 150 F/g. This quickly changes as the current density rises, and at 10 A/g the capacities are 16 F/g, 21 F/g, 57 F/g, and 102 F/g for the s, m, L, and XL-HPCs, respectively. Figure 4e displays the capacity retention trend as the current density rises for the HPCs. Specifically, XL-HPC, with its large pore size distribution, experiences an 65% rate retention relative to a 10% retention for the s-HPC at a loading of 15 mg/cm^2 and current density of 10 A/g. Even the L-HPC begins to show significant fading at this current density; although it is still superior to the smaller pore size HPCs. Once again, XL-HPC shows the best performance at high loading with capacities of 156 F/g and 102 F/g at 0.5 A/g and 10 A/g, respectively. The decreased rate performance as compared to the lower loading samples is due to the increased ion transfer distance.[6,30]

Figure 4f highlights the loading performance of the HPCs. This plot clearly shows how the loading of the sample is detrimental to the s-HPC and m-HPC at 10 A/g. XL-HPC and L-HPC are able to maintain their capacities even at high mass loadings, as seen from the shallow slope of the mass loading curves. The s & m-HPC quickly lose capacity, as ion conduction becomes restricted at high loading in these pore size regimes. The high capacity retention at both high loading and high rate is attributed to the very large pores allowing for efficient mass transport and ion diffusion in the sample.[4,23,31,32] This is especially important for ionic liquids that lack high ionic conductivity.[3] Even though XL-HPC has the lowest surface area, it's huge pore size allows both easier ion conduction as well as better pore accessibility. Volumetric capacities show a similar dependence with the mass loading. At low rate (1 A/g), all HPCs having a relatively constant volumetric capacity over all loadings; on the other hand, at high rate (10 A/g), only XL-HPC maintains a nearly constant volumetric capacity with increasing mass loading, while all other materials show considerable degradation in volumetric capacities at high mass loading due to charge transport limitations (Figure S3a,b).

Specific capacity normalized by the mass of the active material isn't the best way to evaluate the performance of EDLC, particularly at low mass loading where the passive components make up a large fraction of the total mass in the device. For practical applications, the areal capacity could be a more appropriate parameter to evaluate the practical performance of EDLCs, since all passive components are largely constant in a given area.[33] At a low current density of 0.5 A/g, there is barely any difference in areal capacity for all the HPC samples (Figure 5a). There is a clear linear trend between areal capacity and mass loading at this current density. High values above 2 F/cm^2 are achieved for each HPC at loadings of ~ 15 mg/cm^2, with XL-HPC having the highest at 2.27 F/cm^2. These values are quite high for EDLCs with ionic liquid electrolytes, and rival that of aqueous based electrolytes.[4,34,35] At high current densities the HPCs show substantially different behavior with increasing mass loading (Figure 5b). The linear trend disappears, indicating severe ion transport limitations in thick electrode at high current density. The s-HPCs areal capacity shows no increase, indicating the higher material loading is completely offset by the capacity loss due to the transport limitations. There is an initial increase in the areal capacity of m-HPC, however at high loadings of 15 mg/cm^2, the resistance and transport limitations outweigh the benefit of the higher loading. A similar trend is observed for L-HPC; however, the areal capacity decay is much less. Only at the extreme pore size distribution of XL-HPC is there no areal capacity decay with increased mass loading. A high value of 1.48 F/cm^2 is achieved at 10 A/g for this material. Similar to the gravimetric capacitance, the areal capacity is severely impacted by the hierarchical pore size distribution in the HPCs. The larger pores allow for more efficient ion diffusion, even in thick electrodes at both low and high current densities. This is crucial for industrial scale applications where thick electrodes are necessary.

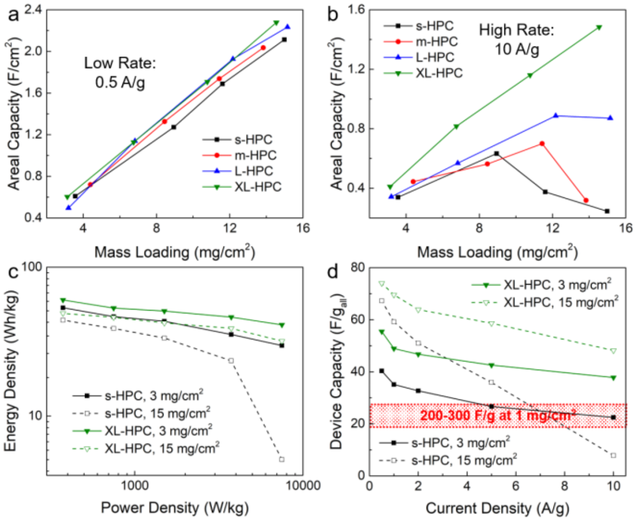

Figure 5. The areal performance at 0.5 A/g (a) and 10 A/g (b) for each HPC. Significant capacity decay is observed for high rate samples, however XL-HPC shows limited fading. Ragone plots (c) of s-HPC and XL-HPC at high and low loadings. Gravimetric capacitance is normalized by the overall total weight of the device, giving values of device capacity (d). Devices with high gravimetric capacities but low loading are incorporated to show where they fall in terms of device capacitance.

A Ragone plot for both high and low mass loading s-HPC and XL-HPC are presented in Figure 5c. The highest energy density and power density achieved were 60.2 Wh/kg and 7500 W/kg, respectively. These values are consistent with other carbon based materials using ionic liquid electrolytes.[3,27,28] However, it is noteworthy that values of 48.9 Wh/kg at 375 W/kg are achieved with a mass loading of 15 mg/cm^2; a loading that is 5-15 times higher than that of most literature values. Furthermore, at a power of 7500 W/kg the energy only decreases to 31.8 Wh/kg, indicating high energy retention. Ragone plots do not account for material loading, so comparable energy and power densities at such high loadings is impressive. The volumetric Ragone plot shows a similar trend as well (Figure S3c).

Figure 5d takes the mass of the passive components into the gravimetric capacity calculation. This is another way to factor in mass loading similar to areal capacity. A value of 10 mg/cm^2 is chosen for the inert components (a mass loading comparable to common current collectors).[32] Many EDLC materials in literature can reach up to 200 F/g, and some over 300 F/g at low mass loadings.[2,5,31] However, the loading of many of these materials rarely exceed 1 mg/cm^2. When weighted by the total device, these capacities drop dramatically (red shaded region in Figure 5d). For example, a device with a capacity of 300 F/g at 1 mg/cm^2 has a device capacity of 27 F/g$_{all}$ assuming a 10 mg/cm^2 loading for inert components. Even with the lowest loading of the s-HPC (3 mg/cm^2) the device capacity reaches a comparable 35 F/g$_{all}$ at 1 A/g. However, with a higher loading these values are increased greatly. Both of the 15 mg/cm^2 HPCs show high device capacities at low rates, however s-HPC exhibits a sharp drop in device capacity as the rate is increased, eventually dropping well below that of conventional EDLCs. On the other hand, XL-HPC shows high device capacities of 74 F/g$_{all}$ and 48 F/g$_{all}$ at current densities of 0.5 A/g and 10 A/g, exhibiting outstanding loading and rate performance. The large hierarchical pore size distribution of XL-HPC is crucial for maintaining a high rate and high capacity at high loading.

Electrochemical impedance spectroscopy provides further insight into the excellent performance of HPCs. Nyquist plots of the HPCs are displayed in Figure 6a. The semicircles for each plot decreases with increasing pore size. This region represents the bulk electrolyte resistance; the larger the semicircle the greater the resistance.[36] Similar phenomena have been reported with ionic liquids with varying pore sizes.[25] A decrease in bulk electrolyte resistance is thought to represent an increase in ion mobility.[25] The trend reinforces the GCD data that larger pores allow for enhanced pore accessibility.

The diffuse layer resistance (Figure 6b inset) is represented by the part of the Nyquist plot that has a 45°, before the sharp increase in slope. This region indicates non-faradaic processes, and can be used to calculate the resistance of the electrolyte in the pores, termed R_{ion}.[32,37,38] A simulation was used to determine the semicircle region to get an accurate value for the 45° region for R_{ion} calculations. Ion resistance is shown to decrease with increasing pore size. This trend, combined with the bulk electrolyte results, indicate that the large hierarchical porosity in the HPCs enable high ion mobility and charge transfer during cycling, granting high rate and loading capabilities.

Conclusion. The relationship between the pore size and distribution of a material and its effect on EDLCs is complex. Hierarchical porous carbon with high nitrogen content, derived from covalent triazine frameworks, was explored as a potential energy storage material in this study. Unique pore structures were synthesized, with various levels of porosity; termed small, medium, large, and extra-large. It was found that the solvent, molten $ZnCl_2$, was responsible for introducing mesoporosity into the sample by acting as a porogen. Weak intermolecular forces between the solvent and solute allow the $ZnCl_2$ to occupy large volumes in-between growing CTF layers during the high temperature synthesis. This leads to large amounts of $ZnCl_2$ producing successively larger pores. This can be disrupted by stronger bonding motifs like pyridines, which prohibit mesopores formation.

Capacities attained were consistent with current EDLCs using ionic liquids with a maximum of 192 F/g at 0.5 A/g. However, HPCs displayed superior areal capacities up to 2.27 F/cm^2 due to heightened pore accessibility and ion mobility which was confirmed by EIS measurements. When normalized by the total device weight, HPCs outperformed other materials with an impressive 74 F/g$_{all}$ vs 27 F/g$_{all}$ of an idealized capacitor material (300 F/g at 1 mg/cm^2). Mass loading is not a common parameter investigated in EDLCs, however it is crucial for the development, and implantation of real life devices.[33] Herein, HPCs are displayed to have tunable hierarchical porosities with excellent electrochemical performance. Contrary to current literature, a larger pore size distribution (with some

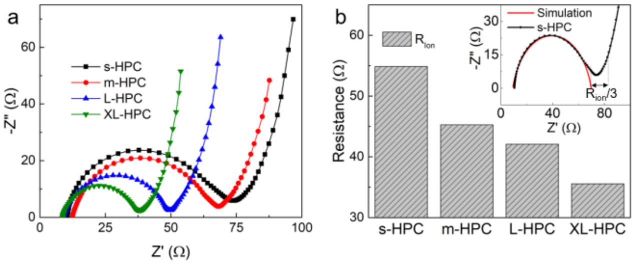

Figure 6. A Nyquist plot of the HPCs with varying pore sizes (a). The semicircle decreases in size with larger pore size HPCs, indicating lower electrolyte resistance. The diffusive resistance in the pores is calculated and found to decrease with increasing pore size (b).

pore volumes being attributed to pore over 50 nm in diameter) is beneficial to EDLCs, especially for high loading and high rate applications.

ASSOCIATED CONTENT

Supporting Information. Additional structural and electrochemical characterizations. This material is available free of charge via the Internet at http://pubs.acs.org.

AUTHOR INFORMATION

Corresponding Author

E-mail: xduan@chem.ucla.edu

Notes

The authors declare no conflict of interest.

ACKNOWLEDGMENT

X.D. acknowledges financial support from National Science Foundation award 1800580.

REFERENCES

(1) Kim, B. K.; Sy, S.; Yu, A.; Zhang, J. Electrochemical Supercapacitors for Energy Storage and Conversion. *Handb. Clean Energy Syst.* **2014**, 1–25. https://doi.org/10.1002/9781118991978.hces112.

(2) Zhong, C.; Deng, Y.; Hu, W.; Qiao, J.; Zhang, L.; Zhang, J. Chem Soc Rev A Review of Electrolyte Materials and Compositions for Electrochemical Supercapacitors. *Chem. Soc. Rev. Chem. Soc. Rev* **2015**, *44*, 7431–7920.

(3) Eftekhari, A. Supercapacitors Utilising Ionic Liquids. *Energy Storage Mater.* **2017**, *9*, 47–69. https://doi.org/10.1016/j.ensm.2017.06.009.

(4) Ni, M.; Huang, Z.; Zhang, X.; Liu, J.; Qiao, L.; Yang, W. Hierarchical Design of Nitrogen-Doped Porous Carbon Nanorods for Use in High Efficiency Capacitive Energy Storage. *RSC Adv.* **2017**, *7*, 22447–22453. https://doi.org/10.1039/c7ra02425h.

(5) Lei, C.; Lekakou, C. Carbon-Based Nanocomposite EDLC Supercapacitors. *Nanotechnol. 2010 Adv. Mater. CNTs, Part. Film. Compos.* **2016**, *1*, 176–179.

(6) Chang, L.; Sun, K.; Hu, Y. H. New Chemistry for New Material: Highly Dense Mesoporous Carbon Electrode for Supercapacitors with High Areal Capacitance. *ACS Appl. Mater. Interfaces* **2018**, *10*, 33162–33169. https://doi.org/10.1021/acsami.8b09661.

(7) Feng, X.; Ding, X.; Jiang, D. Covalent Organic Frameworksw. *Chem. Soc. Rev. Chem. Soc. Rev* **2012**, *41*, 6010–6022. https://doi.org/10.1039/c2cs35157a.

(8) Yaghi, Omar M.; Adrien P. Coˆte, Annabelle I. Benin, N. W. O.; Yaghi, O. M.; Adrien P. Cote´, Annabelle I. Benin, Nathan W. Ockwig, Michael O'Keeffe, Adam J. Matzger, O. M. Y. Porous , Crystalline , Covalent Organic Frameworks. **2005**, *1166*, 1166–1171. https://doi.org/10.1126/science.1120411.

(9) Kim, D. J.; Yoon, J. W.; Lee, C. S.; Bae, Y. S.; Kim, J. H. Covalent Organic Framework-Derived Microporous Carbon Nanoparticles Coated with Conducting Polypyrrole as an Electrochemical Capacitor. *Appl. Surf. Sci.* **2018**, *439*, 833–838. https://doi.org/10.1016/j.apsusc.2018.01.103.

(10) Zhong, S.; Zhan, C.; Cao, D. Zeolitic Imidazolate Framework-Derived Nitrogen-Doped Porous Carbons as High Performance Supercapacitor Electrode Materials. *Carbon N. Y.* **2015**, *85*, 51–59. https://doi.org/10.1016/j.carbon.2014.12.064.

(11) Wang, P.; Wu, Q.; Han, L.; Wang, S.; Fang, S.; Zhang, Z.; Sun, S. Synthesis of Conjugated Covalent Organic Frameworks/Graphene Composite for Supercapacitor Electrodes. *RSC Adv.* **2015**, *5*, 27290–27294. https://doi.org/10.1039/c5ra02251g.

(12) Hao, L.; Ning, J.; Luo, B.; Wang, B.; Zhang, Y.; Tang, Z.; Yang, J.; Thomas, A.; Zhi, L. Structural Evolution of 2D Microporous Covalent Triazine-Based Framework toward the Study of High-Performance Supercapacitors. *J. Am. Chem. Soc.* **2015**. https://doi.org/10.1021/ja508693y.

(13) Kou, Y.; Xu, Y.; Guo, Z.; Jiang, D. Supercapacitive Energy Storage and Electric Power Supply Using an Aza-Fused π-Conjugated Microporous Framework. *Angew. Chemie - Int. Ed.* **2011**, 50, 8753–8757. https://doi.org/10.1002/anie.201103493.

(14) Khattak, A. M.; Ghazi, Z. A.; Liang, B.; Khan, N. A.; Iqbal, A.; Li, L.; Tang, Z. A Redox-Active 2D Covalent Organic Framework with Pyridine Moieties Capable of Faradaic Energy Storage. *J. Mater. Chem. A* **2016**, *4*, 16312–16317. https://doi.org/10.1039/c6ta05784e.

(15) Kuhn, P.; Antonietti, M.; Thomas, A. Porous, Covalent Triazine-Based Frameworks Prepared by Ionothermal Synthesis. *Angew. Chemie - Int. Ed.* **2008**, *47*, 3450–3453. https://doi.org/10.1002/anie.200705710.

(16) Kuhn, P.; Thomas, A.; Antonietti, M. Toward Tailorable Porous Organic Polymer Networks: A High-Temperature Dynamic Polymerization Scheme Based on Aromatic Nitriles. *Macromolecules* **2009**. https://doi.org/10.1021/ma802322j.

(17) Deng, Y.; Xie, Y.; Zou, K.; Ji, X. Review on Recent Advances in Nitrogen-Doped Carbons: Preparations and Applications in Supercapacitors. *J. Mater. Chem. A* **2015**, *4*, 1144–1173. https://doi.org/10.1039/c5ta08620e.

(18) SING, K. S. W.; EVERETT, D. H.; HAUL, R. A. W.; MOSCOU, L.; PIEROTTI, R. A.; ROUQUEROL, J.; SIEMIENIEWSKA, T. REPORTING PHYSISORPTION DATA FOR GAS/SOLID SYSTEMS with Special Reference to the Determination of Surface Area and Porosity. *Pure Appl. Chem.* **1985**, *57*, 603–619. https://doi.org/10.1351/pac198557040603.

(19) Kuhn, P.; Su, D.; Thomas, A. From Microporous Regular Frameworks to Mesoporous Materials with Ultrahigh Surface Area: Dynamic Reorganization of Porous Polymer Networks. *J. Am. Chem. Soc.* **2008**, *130*, 13333–13337. https://doi.org/10.1021/ja803708s.

(20) Artz, J.; Delidovich, I.; Pilaski, M.; Niemeier, J.; Kübber, B. M.; Rahimi, K.; Palkovits, R. Sulfonated Covalent Triazine-

Based Frameworks as Catalysts for the Hydrolysis of Cellobiose to Glucose. *RSC Adv.* **2018**, *8*, 22392–22401. https://doi.org/10.1039/c8ra04254c.

(21) Schwan, J.; Ulrich, S.; Batori, V.; Ehrhardt, H.; Silva, S. R. P. Raman Spectroscopy on Amorphous Carbon Films. *J. Appl. Phys.* **1996**, *80*, 440–447. https://doi.org/10.1063/1.362745.

(22) Ferrari, A. C. Raman Spectroscopy of Graphene and Graphite: Disorder, Electron-Phonon Coupling, Doping and Nonadiabatic Effects. *Solid State Commun.* **2007**, *143*, 47–57. https://doi.org/10.1016/j.ssc.2007.03.052.

(23) Zhang, X. Q.; Dong, W.; Lu, A. H.; Li, W. C. Rational Design of Mesoporous Carbon Electrodes with High Mass Loading for Binder-Free Supercapacitors. *Energy Technol.* **2015**, *3*, 234–241. https://doi.org/10.1002/ente.201402161.

(24) Kuhn, P.; Antonietti, M.; Thomas, A. Porous, Covalent Triazine-Based Frameworks Prepared by Ionothermal Synthesis**. https://doi.org/10.1002/anie.200705710.

(25) Noofeli, A.; Hall, P. J.; Rennie, A. J. R. Ionic Liquid Based EDLCs: Influence of Carbon Porosity on Electrochemical Performance. *Faraday Discuss.* **2014**, *172*, 163–177. https://doi.org/10.1039/c4fd00057a.

(26) Kim, C. H.; Wee, J. H.; Kim, Y. A.; Yang, K. S.; Yang, C. M. Tailoring the Pore Structure of Carbon Nanofibers for Achieving Ultrahigh-Energy-Density Supercapacitors Using Ionic Liquids as Electrolytes. *J. Mater. Chem. A* **2016**, *4*, 4763–4770. https://doi.org/10.1039/c5ta10500e.

(27) Zhou, D.; Wang, H.; Mao, N.; Chen, Y.; Zhou, Y.; Yin, T.; Xie, H.; Liu, W.; Chen, S.; Wang, X. High Energy Supercapacitors Based on Interconnected Porous Carbon Nanosheets with Ionic Liquid Electrolyte. *Microporous Mesoporous Mater.* **2017**, *241*, 202–209. https://doi.org/10.1016/j.micromeso.2017.01.001.

(28) Tran, C.; Lawrence, D.; Richey, F. W.; Dillard, C.; Elabd, Y. A.; Kalra, V. Binder-Free Three-Dimensional High Energy Density Electrodes for Ionic-Liquid Supercapacitors. *Chem. Commun.* **2015**, *51*, 13760–13763. https://doi.org/10.1039/c5cc04359j.

(29) Yao, B.; Chandrasekaran, S.; Zhang, J.; Xiao, W.; Qian, F.; Zhu, C.; Duoss, E. B.; Spadaccini, C. M.; Worsley, M. A.; Li, Y. Efficient 3D Printed Pseudocapacitive Electrodes with Ultrahigh MnO 2 Loading. *Joule* **2019**, *3*, 459–470. https://doi.org/10.1016/j.joule.2018.09.020.

(30) Maiti, U. N.; Lim, J.; Lee, K. E.; Lee, W. J.; Kim, S. O. Three-Dimensional Shape Engineered, Interfacial Gelation of Reduced Graphene Oxide for High Rate, Large Capacity Supercapacitors. *Adv. Mater.* **2014**, *26*, 615–619. https://doi.org/10.1002/adma.201303503.

(31) Sun, H.; Zhu, J.; Baumann, D.; Peng, L.; Xu, Y.; Shakir, I.; Huang, Y.; Duan, X. Hierarchical 3D Electrodes for Electrochemical Energy Storage. *Nat. Rev. Mater.* **2019**, *4*, 45–60. https://doi.org/10.1038/s41578-018-0069-9.

(32) Sun, H.; Mei, L.; Liang, J.; Zhao, Z.; Lee, C.; Fei, H.; Ding, M.; Lau, J.; Li, M.; Wang, C.; et al. Three-Dimensional Holey-Graphene/Niobia Composite Architectures for Ultrahigh-Rate Energy Storage. *Science.* **2017**, *356*, 599–604. https://doi.org/10.1126/science.aam5852.

(33) Gallagher, K. G.; Trask, S. E.; Bauer, C.; Woehrle, T.; Lux, S. F.; Tschech, M.; Lamp, P.; Polzin, B. J.; Ha, S.; Long, B.; et al. Optimizing Areal Capacities through Understanding the Limitations of Lithium-Ion Electrodes. *J. Electrochem. Soc.* **2015**, *163*, A138–A149. https://doi.org/10.1149/2.0321602jes.

(34) Ma, X.; Zhao, L.; Yu, Z.; Wang, X.; Song, X.; Ning, G.; Gao, J. Excellent Compatibility of the Gravimetric and Areal Capacitances of an Electric-Double-Layer Capacitor Configured with S-Doped Activated Carbon. *ChemSusChem* **2018**, *11*, 3766–3773. https://doi.org/10.1002/cssc.201801767.

(35) Zhi, L.; Li, T.; Yu, H.; Chen, S.; Dang, L.; Xu, H.; Shi, F.; Liu, Z.; Lei, Z. Hierarchical Graphene Network Sandwiched by a Thin Carbon Layer for Capacitive Energy Storage. *Carbon N. Y.* **2017**, *113*, 100–107. https://doi.org/10.1016/j.carbon.2016.11.036.

(36) Mei, B. A.; Munteshari, O.; Lau, J.; Dunn, B.; Pilon, L. Physical Interpretations of Nyquist Plots for EDLC Electrodes and Devices. *J. Phys. Chem. C* **2018**, *122*, 194–206. https://doi.org/10.1021/acs.jpcc.7b10582.

(37) Ogihara, N.; Kawauchi, S.; Okuda, C.; Itou, Y.; Takeuchi, Y.; Ukyo, Y. Theoretical and Experimental Analysis of Porous Electrodes for Lithium-Ion Batteries by Electrochemical Impedance Spectroscopy Using a Symmetric Cell. *J. Electrochem. Soc.* **2012**, *159*, A1034–A1039. https://doi.org/10.1149/2.057207jes.

(38) Ogihara, N.; Itou, Y.; Sasaki, T.; Takeuchi, Y. Impedance Spectroscopy Characterization of Porous Electrodes under Different Electrode Thickness Using a Symmetric Cell for High-Performance Lithium-Ion Batteries. *J. Phys. Chem. C* **2015**, *119*, 4612–4619. https://doi.org/10.1021/jp512564f.

ToC Figure:

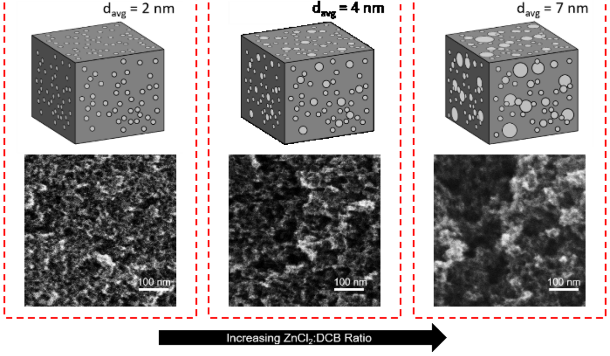
d_{avg} = 2 nm
d_{avg} = 4 nm
d_{avg} = 7 nm
100 nm
100 nm
100 nm
Increasing $ZnCl_2$:DCB Ratio